Bio-Design and Manufacturing (2023) 6:536–549
https://doi.org/10.1007/s42242-023-00254-2

RESEARCH ARTICLE

Proof of concept of a self-tightening needle-less suture using a NiTi shape memory alloy

Adelaide Nespoli[1] · Davide Ninarello[1] · Enrico Bassani[1] · Villiam Dallolio[2]

Received: 9 January 2023 / Accepted: 25 June 2023 / Published online: 17 August 2023

Abstract

Among surgical procedures, suturing is considered simple. However, in some situations, suturing is not easy or feasible. Here, we present proof of concept of a new self-tightening needle-less suture made of a NiTi alloy. The new device is designed to overcome two demanding steps of traditional suturing: needle introduction and manual knotting. Our novel suture is composed only of a short NiTi wire that is able to change shape by exploiting a thermoelastic phase transition. This shape change is achieved by increasing the temperature from that of the operating room (e.g., 20–22 °C) to 32 °C using warm water. Suturing consists of two steps: suture introduction, in which the suture is in an open configuration, and shape recovery (i.e., closed configuration). The closed configuration is maintained at human body temperature thanks to peculiar pseudoelastic properties of the NiTi material. Finally, thermal and functional characterization verified the simplicity and effectiveness of the proposed device.

Graphic abstract

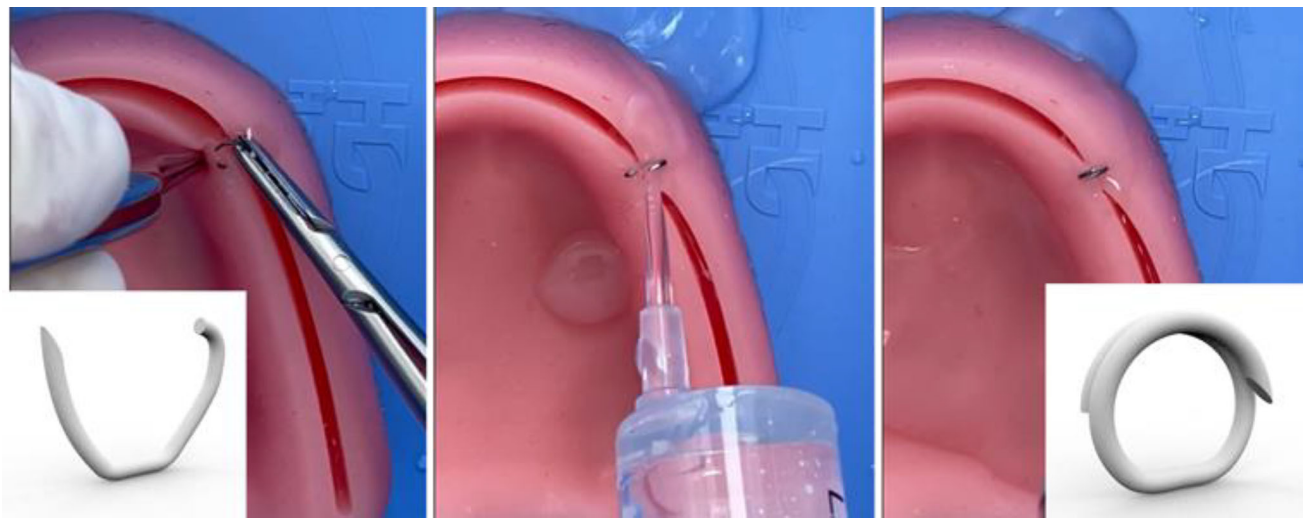

Keywords Suture · NiTi · Shape memory alloys · Suturing · Medical device

Introduction

Surgical sutures are employed to ligate blood vessels and to connect tissues together; to date, it is the most widely used medical device. Sutures consist of a thread with a metal needle attached to one side. At present, different types

✉ Adelaide Nespoli
adelaide.nespoli@cnr.it

1 Institute of Condensed Matter Chemistry and Technologies for Energy, National Research Council (CNR-ICMATE), 23900 Lecco, Italy

2 Promev Srl, 23900 Lecco, Italy

of sutures are available, and these are classified according to the material of the thread (i.e., absorbable versus non-absorbable, synthetic versus natural) and the structure (i.e., monofilament, multifilament, twisted, or braided). Surgical needles are manufactured using many types of alloys, including different types of martensitic stainless steel (i.e., S42000, S42020, and S45500), austenitic stainless steel (316L), and plated carbon steels. Proprietary needle alloys with higher amounts of nickel and molybdenum have also been developed (i.e., Surgalloy and Ethalloy). These materials have many desirable characteristics, including corrosion resistance, strength, and ductility [1, 2]. Needles may be straight or curved with round or triangular cross sections. In general, the choice of suture and needle depends on clinical variables, including the location, the thickness of the tissue, and the amount of tension exerted on the wound [3].

Suturing consists of multiple manual knots that may run continuously or separately. The suturing procedure is not easy and may not be possible in all clinical scenarios. Maintaining adequate tension while tying the knot is a main issue during suturing. Too much tension can cause the suture or tissue to break, while insufficient tension can cause the knot to fail. The failure rate of suturing is both high and variable, especially in procedures involving deep tissues. Suturing can be demanding and requires long medical intervention time when the surgical field is difficult to access, as in endoscopic skull base surgery, laparoscopic myomectomy, and minimal invasive esophagectomy. Studies of post-surgical issues with endoscopic skull base surgery have reported that as much as 7.1% of cerebrospinal fluid was leaked following tumor resection via the endoscopic endonasal skull base approach [4]. Postoperative cerebrospinal fluid leakage incidence was also studied by Xue et al. [5], who found a 12.7% loss rate, as well as Malik et al. [6], who reported estimates ranging from 1.77% to 7% for cerebrospinal fluid fistulas, and Chen et al. [7], who reported a cerebrospinal fluid leakage incidence of 15.48%. Additional research has found that postoperative cerebrospinal fluid rhinorrhea remains a frequent complication of endonasal approaches to pituitary and skull base tumors, with an incidence rate varying from 3.7% to 9%, depending on the approach adopted [8].

Laparoscopic myomectomy (LM) is the main intervention used to treat uterine myomas, a type of tumor involving uterine muscle cells that can lead to significant morbidity and fertility problems [9, 10]. LM is performed totally laparoscopically and requires intracorporeal suturing, increasing the difficulty of the procedure. Typically, sutures under 30 cm are introduced through the port into the intraperitoneal cavity. Although difficult, it is important to ensure that no hematomas form in the myoma beds. Suturing is one of the most important factors affecting the outcome of this procedure, with the hardest part consisting of tying suture knots [11, 12]. Similarly, appropriate suturing procedures are fundamental for minimally invasive surgeries such as esophagectomies. The thoracic esophagus is proximate to many sensitive surrounding structures, and therefore, the procedure must be as precise and as little invasive as possible. One of the key factors determining the success of minimally invasive esophagectomy procedures is the anastomotic technique. Anastomotic leakage is a critical complication of this procedure and can lead to patient death [13]. The esophagogastric anastomosis is secured by manual or mechanical techniques. Manual techniques usually involve absorbable or non-absorbable sutures, while the mechanical supports are usually staple sutures. While cervical anastomosis is mainly performed using a handsaw, intrathoracic anastomosis is usually performed using staple sutures, since manual suturing would require considerable technical skills and be highly time-consuming [14]. However, studies have reported a 20% incidence of anastomosis stenosis after the use of staple sutures for this procedure, meaning that the optimal surgical plan remains an unsolved problem [15].

In addition to the examples mentioned above, other complications associated with suturing are critical and may lead to serious medical problems. Partial or complete dehiscence, infection without dehiscence, and suture reaction are additional risks that apply to both deep and superficial suturing. These risks can increase both morbidity and mortality, prompt transfer to an intensive care unit setting, result in longer hospitalization, and may cause hospital readmission [16]. For example, abdominal wound dehiscence (i.e., burst abdomen or fascial dehiscence) is a severe postoperative complication, with a mortality rate as high as 45% and an incidence ranging from 0.4% to 3.5% of cases [17]. Furthermore, infection in post-cesarean wounds and independent risk factors related to wound infection have been studied [18]. Such studies have found that the overall incidence of wound dehiscence was 3.05%, with all patients requiring secondary suturing.

In general, in cases of suture failure, the best-case clinical situation is re-suturing. However, the worst-case scenarios often involve patient death. Regardless of the specific suture and needle selected, the basic techniques of suturing—i.e., holding the needle, driving the needle, and knot placement—remain the same. Traditional suturing involves the following steps: (1) needle introduction, (2) manual knotting with suturing instruments, and (3) cutting of the excess thread. In traditional suturing, the difficulty, time, and risk assessment are the main constraints (Table 1). Manual knotting is the most critical step for two main reasons. First, it always involves multiple knots, and second, its effectiveness is surgeon-dependent since its success is related to operator skill. Furthermore, knotting may be even more difficult in confined spaces, resulting in even longer intervention times. The needle introduction step also presents high levels of risk

Table 1 Risk assessment of traditional surgical suturing by surgical step

Surgical step	Difficulty level	Time	Risk
Needle introduction	Low	Low	High
Knotting	High	High	High
Cutting	Low	Low	Low

due to the possibility of accidental puncture of adjacent tissues by the operator. This may result in increased risk of infection and therefore in waste of medical material due to the additional treatment required. Finally, needle introduction can also result in the widening of the hole through which the suture is passed, and this can considerably increase the risk of infection—especially in neurosurgery—and can reduce suture strength.

Surgical site infections are a dramatic side effect of suturing and impact both patients and medical staff [19]. Infections result from microbial infiltration via the knot or the needle and can lead to additional undesirable effects such as legal disputes and needle disposal. Even without infection, the manual knotting step has a strong impact on the surgeon, especially during operations featuring prolonged suturing sessions. Manual knotting also impacts patients, since longer anesthesia periods are required. Furthermore, these factors all result in increased surgery costs.

Thus, considering the impact of risk assessment, infection, and cost/efficiency, a new suturing procedure or suturing device must face two key challenges: improvement of needle introduction and improvement of knotting while abolishing the cutting phase. Biomedical research has reported many new materials to remove suture knots, particularly in confined space. An example is the barbed suture. Barbed sutures are derived from common polymeric sutures, but their surface is cut to generate numerous sharp barbs that give sutures tensile strength without the need for tying, thereby favoring self-anchoring [20, 21]. A comprehensive review of the efficacy and safety of knotless barbed sutures for surgery is provided by Lin et al. [22]. In that review, the authors concluded that this kind of suture is effective for reducing suturing and total operative time, even if additional safety evidence is required. Furthermore, the usefulness of the barbed sutures for deep and narrow operations remains unknown.

Another proposal to remove the knotting step is reported by Nespoli et al. [23]. They presented an innovative suture based on a shaped NiTi wire that closes automatically when heated. NiTi is the most common shape memory alloy and has been used in numerous industrial applications due to its unique mechanical properties, including the shape memory effect (SME) and pseudoelasticity (PE). In addition, NiTi wires show high resistance to damping and fatigue, high resistive strength, good biocompatibility, and high corrosion resistance. Major uses of NiTi are in medicine (e.g., as stents, grafts, orthopedic staples, orthodontic archwires, and eyeglass frames), aerospace (e.g., as couplers in F-14 planes), safety products (e.g., as dampers of seismic vibrations and as sprinklers), and robotics (e.g., as actuators) [24–33]. At the base of the mechanical attitudes of NiTi, there is a first-order thermoelastic transition between two solid phases, austenite and martensite, that are stable at two different temperatures. Austenite is the parent phase; it has a body-centered cubic structure and is stable at high temperatures. Martensite is softer and is stable at low temperatures but can exist in multiple variants due to its low symmetry. An additional martensite phase with a trigonal cell, called the R-phase, may also appear to generate a two-step transformation. Thermoelastic martensitic transition (TMT) is characterized by thermal and mechanical hysteresis, and growth and shrinking of martensite upon cooling and heating [34]. This appears following the martensitic transformation (SME or PE) and is governed by the characteristic transformation temperatures of the alloys: the martensite start and finish temperatures, M_s and M_f, and the austenite, or reverse transformation start and finish temperatures, A_s and A_f.

The SME occurs when a specimen, deformed at a temperature below M_f, recovers its original undeformed shape when heated to a temperature above A_f. The motion produced through the phase change from martensite to austenite and vice versa can thus be exploited to produce mechanical work; it is for this reason that NiTi is valuable in the actuation field. On the other hand, PE occurs in the austenite state. At low strains, the austenite first behaves like a common elastic material. However, when reaching a critical level of stress, austenite transforms into a stress-induced martensite (SIM). The transition into SIM produces high deformation at almost constant load due to the high mobility of the interfaces of martensite variants; this minimizes strain energy. Importantly, SIM is thermodynamically unstable at austenite temperatures. Therefore, when the load is removed, the material returns to the austenitic parent phase following an unloading path at lower stresses than the initial load stress. This means that PE is a reversible, nonlinear elastic phenomenon [34]. It is important to note that PE may only appear in the well-known pseudoelastic temperature range from A_f to M_d, where M_d is the temperature above which martensite can no longer be induced by stress and the material shows a purely austenitic mechanical response.

Characteristic PE curves can show a "flag" shape, which is typical of strongly textured specimens such as wires, or a "leaf" shape, which is common for more complex geometries. In both cases, thermo-mechanical hysteresis can be very attractive for practical applications since it can help dissipate mechanical energy and prevent or reduce structural damage due to vibrations.

In [23], the authors presented a ring-like NiTi suture that presented the SME in the operating room and the PE at human body temperature. These NiTi sutures were able to change their shape from an open to a closed configuration solely via change in temperature. Therefore, in this case, suture tying is not operator-dependent since knotting is substituted by spontaneous shape recovery via exposure to heated water. Such a design may be useful in deep surgical field where manual knotting is very challenging, or even impossible. The suture described in the aforementioned paper [23] has a similar shape to traditional sutures, but it is composed of a pre-shaped NiTi wire with a steel needle crimped on one side. Using this NiTi device, the suturing steps changed to: (1) needle introduction, (2) wire positioning, (3) cutting of excess thread, and (4) closing the knot by applying heated water. Therefore, the suturing procedure involving NiTi sutures faces only one challenging step: the introduction of the needle.

In this paper, we suggest a further improvement to the previously described NiTi suture [23] by presenting a needle-free design of a similar NiTi-based suture [35]. This design radically reduces the demanding steps involved in suturing since the procedure involves only wire introduction and knot self-closure with heated water. The presented device is a proof of concept, and it has been assessed at a technology readiness level of four, meaning that it was validated in a laboratory environment.

Materials and methods

Suture design

Our objective was to develop a user-friendly NiTi-based suture with simple geometry, needle-free and following a previously published shape [35]. Since the advantage of using the NiTi material is the possibility of exploiting temperature-sensitive shape changes, the proposed NiTi suture is designed to have two shapes, i.e., an open geometry at operating room temperature and a closed one at human body temperature, respectively. These configurations were chosen to meet two goals: the open configuration facilitates introduction of the device into tissues, while the closed configuration (i.e., a single-loop spring) facilitates simplicity of fabrication and improves biocompatibility. Relative to the traditional approach (Table 1), the new suturing operation becomes simpler since it reduces to two steps: (1) wire introduction and (2) closure of the knot with warm water. Figure 1 depicts a three-dimensional computer-aided design (CAD) model of the suture in each configuration.

The device features two geometrical parameters, Φ_S and Φ_W, which are the diameters of the closed suture and the NiTi wire, respectively. The length of the NiTi wire, L_W, is kept at 1.5 times the circumference of the suture. Furthermore, the sharp tip of the suture facilitates introduction into human tissue, while the curved end acts as a mechanical stop. In addition, the suture is designed to have a straight segment to make it easy for surgical instruments to grasp.

Suture fabrication and characterization

A body-temperature cold-worked NiTi wire with a diameter of 0.4 mm (Φ_W) was purchased from SAES Getters (Italy). Three suture types with Φ_S of 2 mm (Φ_{S2}), 3 mm (Φ_{S3}), and 4 mm (Φ_{S4}) were fabricated using three different processing routes. Suture fabrication followed two main medical recommendations: First, the open configuration should be stable at the ambient temperature of the operating room (i.e., approximately 20–22 °C) and second, sutures should close at a maximum temperature between 35 °C and 40 °C. The open-to-closed transition is achieved by heating the device with hot water delivered by a syringe.

The as-received NiTi wires followed a series of thermal treatments at high temperatures (i.e., from 400 to 600 °C) to identify the phase transformation temperature for the NiTi material that best meets the medical requirements. Ad hoc steel jigs were used to fix the closed configuration to the wire during the thermal treatment. The selected thermal treatment procedure to guarantee the correct functioning temperatures as well as the design of the home-made jigs is industrial property.

From a material point of view, the medical temperature constraints require that the suture is in the deformed martensite state (open configuration) until heated with water. Therefore, the suture should start its martensite-to-austenite (i.e., open-to-closed) transition at a temperature higher than 20–22 °C. In addition, the phase transition should finish at an A_f of approximately 35 °C. The closed configuration is then maintained at the human body temperature since the austenite state can be constantly maintained at that temperature. The starting open configuration is obtained during manufacturing via controlled deformation of the suture at a temperature lower than R_f that is the finish temperature of the transition from austenite to the R-phase. The open configuration is obtained by cooling down the treated NiTi and creating the suture opening using a proprietary jig. Therefore, when surgeons receive the NiTi suture in its open configuration, the suturing steps will be: (1) suture introduction and (2) closure of the suture with warm water. Figure 2 shows a visualization of the steps characterizing the lifespan of the NiTi suture from production to use in the operating room.

Differential scanning calorimetry (DSC) (DSC25, TA Instruments, New Castle, DE) was used to assess the phase transformation temperatures of the NiTi material after thermal treatments. Temperature scans were performed on six specimens per type over −90–120 °C at a 10 °C/min heating/cooling rate. Characteristic suture temperatures include

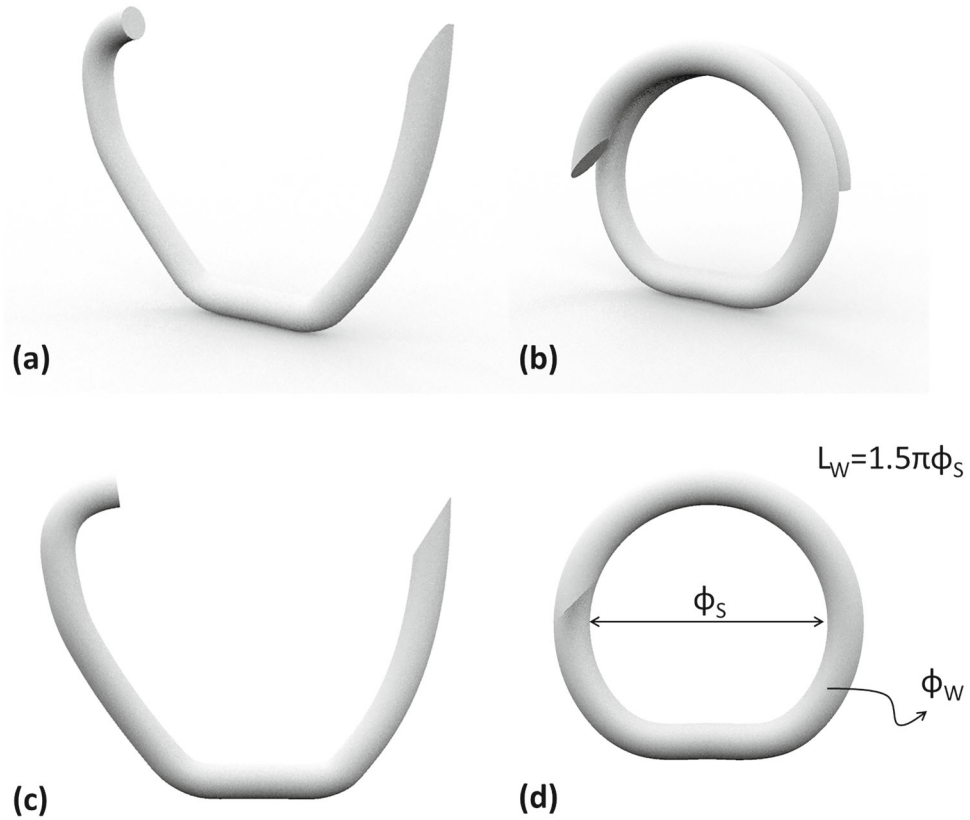

Fig. 1 Three-dimensional computer-aided design (CAD) models of the suture in the open (**a** and **c**) and closed (**b** and **d**) configurations. Φ_S: diameter of the closed suture; Φ_W: diameter of the NiTi wire; L_W: length of the NiTi wire

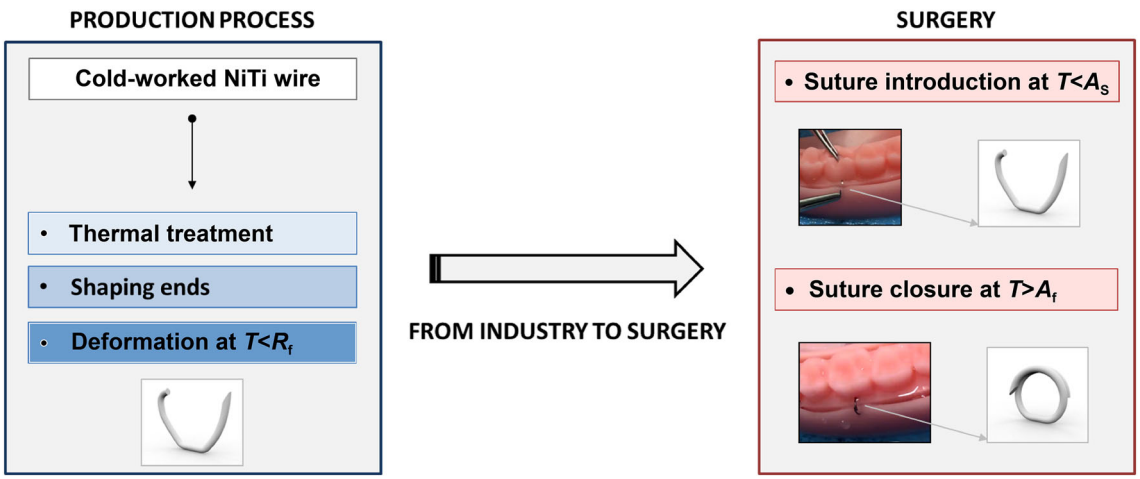

Fig. 2 Life cycle analysis of the novel NiTi suture, from factory to operating room

the maximum temperature at which the suture can be deformed in its open configuration, R_f, and the temperatures at which the transition from open to closed configurations occurs, A_s, A_p, and A_f. A_s is the temperature when open suture starts to close and the closing operation finishes at A_f. A_p is the temperature of the transition peak. All characteristic temperatures, except A_p, are identified in the DSC plot using the tangent method.

A final post-processing step was used to model the two ends. For example, 320-grit abrasive paper was used to sharpen the tip, while pliers were used to give a slight curvature to the other end. The curvature is given to the NiTi device at R-phase temperature; therefore, it is recovered through the phase transformation from the open to the closed configuration.

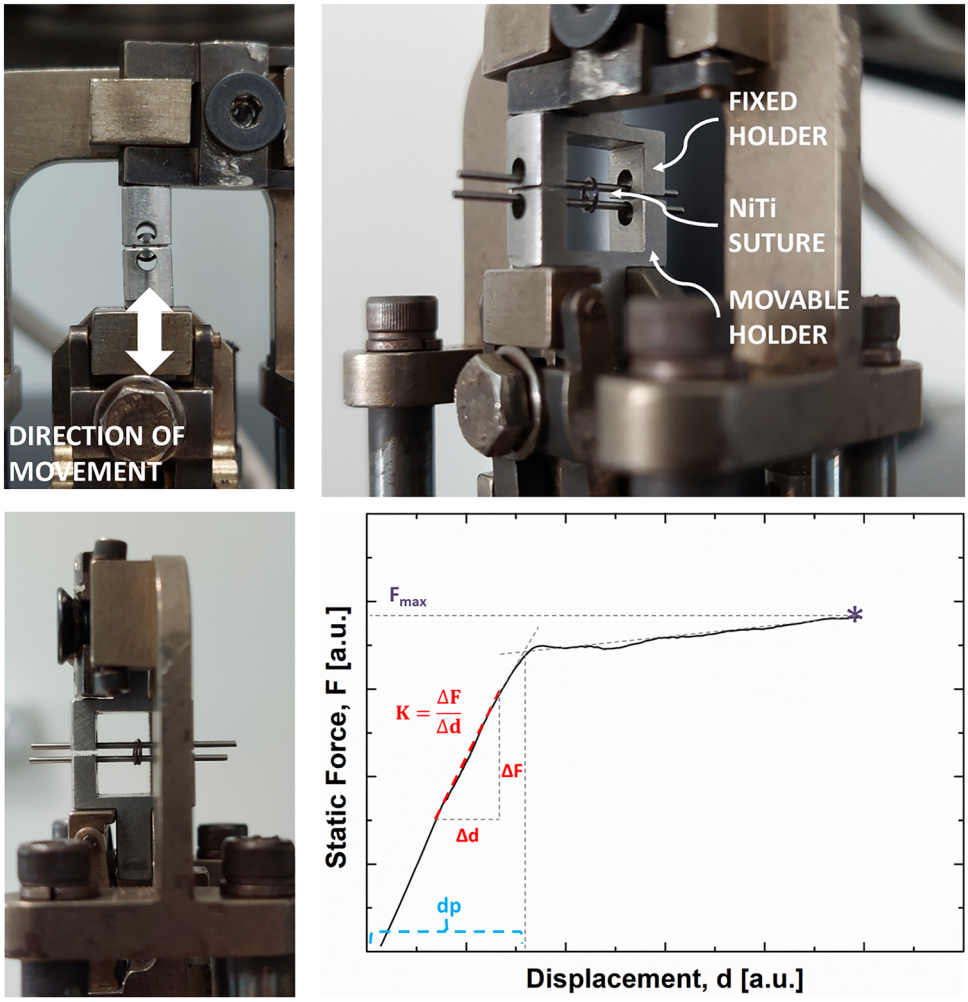

Fig. 3 Photographs of the thermo-mechanical testing setup and main mechanical parameters obtained using a generic force versus displacement graph. K: elastic stiffness; d_p: plateau starting displacement; F_{max}: maximum force (all quantities expressed in arbitrary units)

Thermo-mechanical tests were performed using a Q800 machine (TA Instruments) to assess the opening force of each suture at 37.5 °C and at R_f and to evaluate the closing force generated by the suture during heating above A_f. During all tests, temperatures were measured by a thermocouple placed near the holders. Before mechanical testing of the opening force, the Q800 chamber was maintained at the selected temperature for 10 min. The movement action was transferred to the suture using the ad hoc support depicted in Fig. 3. This support consists of two similar rigid frames fixed to one of the two holders of the tensile strength testing apparatus. The axial movement of the bottom frame permits suture opening (downward movement) and closing (upward movement). To assess its strength at 37.5 °C, each suture was deformed by a complete load–unload cycle at 0.250 mm/min and at four opening levels: 0.500, 0.650, 0.750, and 1 mm. In addition, the assessment of the opening force at R_f was accomplished at 1 N/min and at 1 mm deformation. Curves were then evaluated by three parameters identified on the loading path: the elastic stiffness (K), the plateau starting displacement (d_p), and the maximum force (F_{max}) (Fig. 3).

Next, the closing force of the suture was measured using an iso-displacement test. Each tested suture was first cooled in near-frozen water and then opened as illustrated in Fig. 1. Then, the two extremities were inserted in rigid strips fixed to both the upper and lower clamps of the Q800 testing machine. A distance equal to the one between the two branches of the suture in the open configuration was then set up between the rigid strips. Using optical microscopy (i.e., using a WILD stereomicroscope with light emitting diode (LED) illumination and a polarizer), the distance of the suture branches in the open configuration was measured for all the three suture sizes. For Φ_{S2}, Φ_{S3}, and Φ_{S4}, we recorded distances of 3.4, 5.5, and 7 mm, respectively. Once the opened suture was inserted in the rigid strips, the temperature of the chamber was increased to 45 °C in iso-displacement conditions. During the heat ramp, the force applied by the suture was measured. Using this test, the force plateau value was considered to be the maximum force that the suture can apply to tissues during the closing process. Finally, functional tests were accomplished on silicon anatomical samples and on commercial anatomical animal tissues.

Results

Figure 4 presents photographs of the three sutures—Φ_{S2}, Φ_{S3}, and Φ_{S4}—in both the open and closed configurations. All photographs were taken at room temperature (approximately 23 °C) using a WILD stereomicroscope. Figure 5 shows the DSC graphs of the sutures and also reports the temperature limits for each configuration. The peak at about −70 °C during cooling is not consistent due to the machine losing control of the selected cooling rate. The characteristic temperatures R_f, A_s, A_p, and A_f of the three sutures together with their average values are listed in Table 2. Given the average values, we found that the upper limit of R_f is (15.2±0.8) °C. Moreover, the phase transition temperature limits, A_s and A_f, are (18.2±2.0) and (31.2±0.8) °C, respectively. Next, with respect to the energy involved in the phase transformation, we found that the three sutures had similar enthalpy values: 17.6 J/g (standard deviation (SD): 0.4 J/g), 18.5 J/g (SD: 0.5 J/g), and 17.9 J/g (SD: 0.2 J/g) for sutures Φ_{S2}, Φ_{S3}, and Φ_{S4}, respectively.

Results of the mechanical tests on the opening force of the sutures are reported in Fig. 6 and summarized in Table 3. We observed that at human body temperature, the three sutures showed the well-known pseudoelastic flag-shaped response. The loading path is composed by a linear elastic response followed by a plateau of SIM. Moreover, we observed that the elastic stiffness and maximum force decrease with increasing suture diameter. An opposite trend was found for the SIM plateau starting displacement, which instead increases with the suture diameter. Therefore, we obtained 322.5, 332.7, and 646.8 μm for diameters of 2, 3, and 4 mm, respectively. As expected, at R_f, the material is softer, with stiffness and forces lower than those registered for the austenite state. It should be noted that the mechanical response at R_f was similar for the three sutures. Finally, the closing force measure test showed that the static force exerted by sutures Φ_{S2}, Φ_{S3}, and Φ_{S4} is equal to 2.3, 1.9, and 1.7 N, respectively. It is noted a decrease in the closing force by increasing the diameter of the closed suture.

Finally, we tested suturing on silicon phantoms of human gingivae. Figure 7 depicts frames representing the surgical steps for suture Φ_{S2}: suture introduction (Fig. 7a) and self-knotting (Figs. 7b and 7c). Figure 8 shows the surgical steps for suture Φ_{S3}; these included suture introduction (Figs. 8a and 8b) and self-knotting (Figs. 8c and 8d). Finally, Fig. 9 shows photographs of suture tests on commercial animal samples, carried out using the Φ_{S4} (Figs. 9a–9c) and Φ_{S3} (Figs. 9d–9f) sutures.

Discussion

Here, we present a simple, rational, easy, user-friendly, and cost-effective suture based on a shape memory alloy wire. The NiTi material was chosen to guarantee high biocompatibility that is usually achieved with dedicated post-processing beneficial in promoting a physical barrier for Ni ions (such as oxidation or coating). Furthermore, the material has the extra medical benefit of being magnetic resonance imaging (MRI)-compatible [36]. The suture itself consists of a body-temperature NiTi wire that is hot-shaped into a single-loop ring via ad hoc thermal treatment. These sutures possess a shape memory form (SME) at room temperature and a pseudoelastic form (PE) at human body temperature. The suture is therefore in a deformed martensite state (i.e., an open configuration) during placement within the tissue, where it recovers the ring shape (i.e., a closed configuration) when heated above A_f. The closing movement enables tissue margins to be drawn together and consequently for the sutured wound to close. The coexistence of the SME and PE forms is beneficial in many ways. First, SME allows the suture to keep an open configuration until being exposed to heat. In the PE condition, small thermal fluctuations around typical internal human body temperature [37] do not affect the mechanical performance of the suture since it remains permanently in the austenite state (i.e., the suture is pseudoelastic) inside the human body. This is in accordance with our DSC analysis results. Therefore, any increase or decrease of temperature (either locally or outside the body) does not affect the correct functioning of the suture since the mechanical properties of the material are exclusively related to its austenite microstructure. A production process was selected to promote the SME in a temperature range suitable for standard operating room environment. Our DSC results (Fig. 4 and Table 2) show that the mean value of A_s is (18.2±2.0) °C. Therefore, at laboratory temperature (approximately 23 °C) the device partially recovered the closed shape. Moreover, it kept this configuration even at the surgery temperature since the mean value of A_p was (26.9±0.8) °C.

We also note that the open-to-closed transition always occurs in a narrow temperature range (approximately 10 °C) since the temperature must be increased from 20 to 22 °C to A_f ((31.2±0.8) °C). In addition, the water used to heat the suture can be at a temperature of 38–40 °C to ensure that the phase transition is fast without damaging the surrounding tissue.

At human body temperature, the suture remained in the closed configuration with the PE mechanical response specific for each diameter (Fig. 6 and Table 3). Once closed, the stiffness of the suture is 25.6, 15.9, and 6.5 N/mm for the Φ_{S2}, Φ_{S3}, and Φ_{S4} sutures, respectively. Based on these results, we conclude that at body temperature the new suture

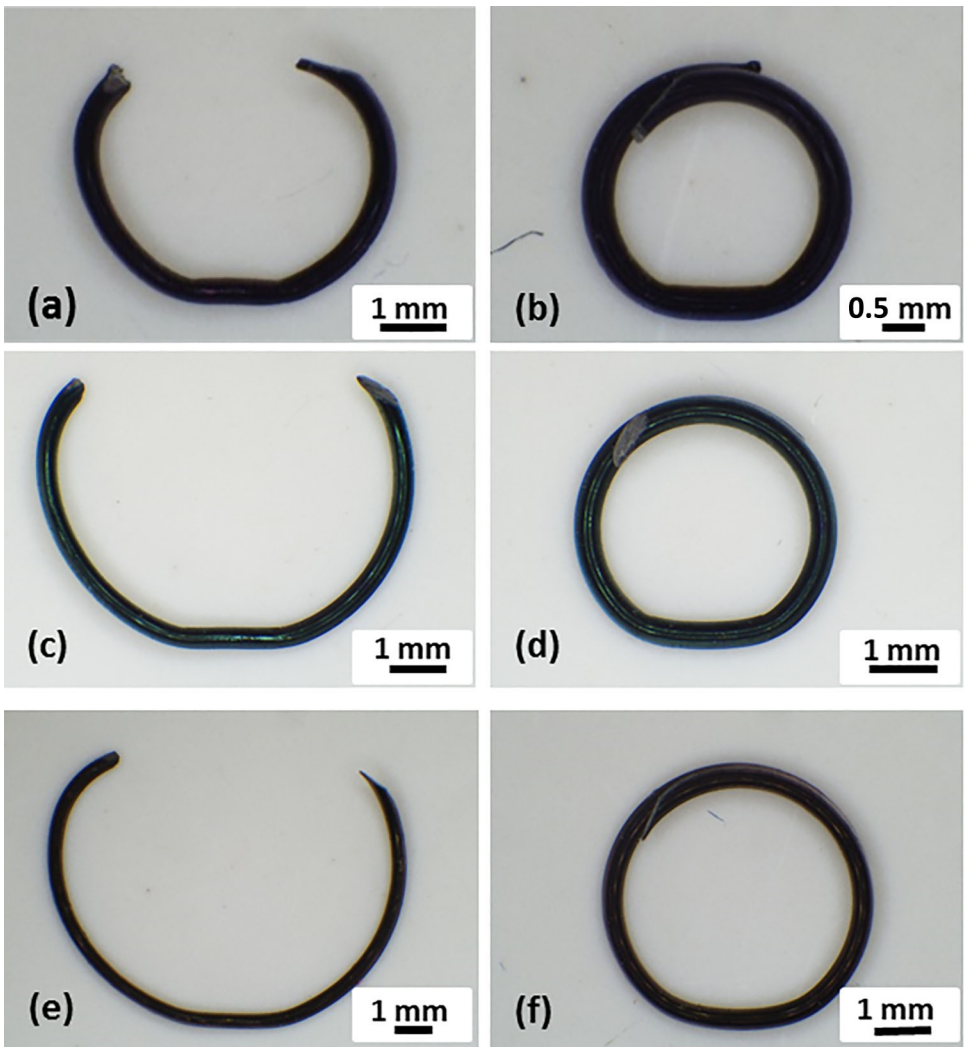

Fig. 4 Photographs of the sutures: Φ_{S2} (**a** and **b**), Φ_{S3} (**c** and **d**), and Φ_{S4} (**e** and **f**). Φ_{S2}: suture with closed configuration diameter of 2 mm; Φ_{S3}: suture with closed configuration diameter of 3 mm; Φ_{S4}: suture with closed configuration diameter of 4 mm

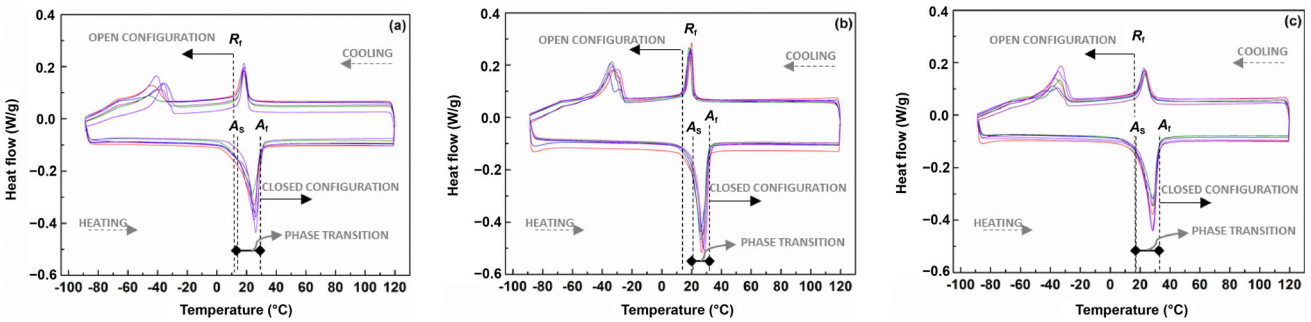

Fig. 5 DSC graphs for the Φ_{S2} (**a**), Φ_{S3} (**b**), and Φ_{S4} (**c**) sutures. R_f represents the upper temperature limit for suture opening. A_s and A_f are the temperature limits at which the open-to-closed transition occurs. DSC: differential scanning calorimetry; Φ_{S2}: suture with closed configuration diameter of 2 mm; Φ_{S3}: suture with closed configuration diameter of 3 mm; Φ_{S4}: suture with closed configuration diameter of 4 mm

Table 2 Characteristic temperatures of the Φ_{S2}, Φ_{S3}, and Φ_{S4} sutures

Suture	R_f (°C)	A_s (°C)	A_p (°C)	A_f (°C)
Φ_{S2}	13.1±0.6	16.1±2.5	25.3±0.9	29.8±0.9
Φ_{S3}	14.9±1.3	20.6±0.9	26.8±1.1	31.0±1.1
Φ_{S4}	17.5±0.6	17.8±2.6	28.6±0.6	32.8±0.3
Mean	15.2±0.8	18.2±2.0	26.9±0.8	31.2±0.8

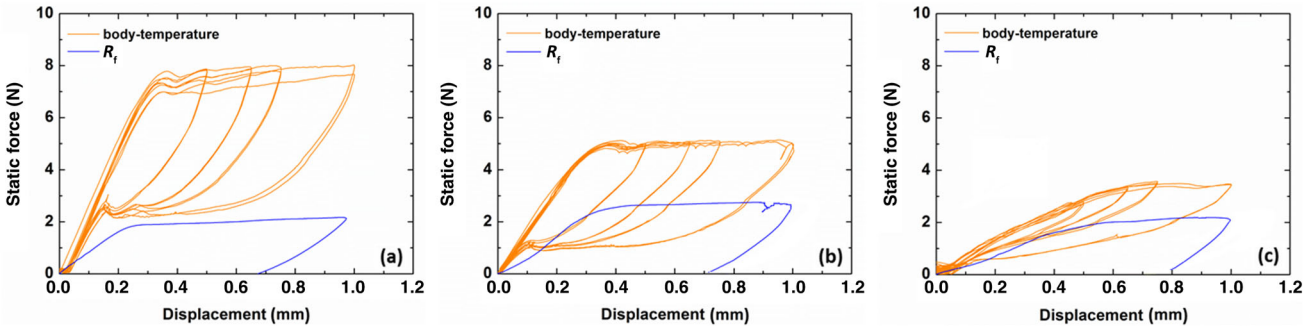

Fig. 6 Loading–unloading mechanical cycle at human body temperature (orange curves) and at R_f (blue curves): **a** suture with a 2-mm diameter; **b** suture with a 3-mm diameter; **c** suture with a 4-mm diameter

Table 3 Elastic stiffness (K), plateau starting deformation (d_p), and maximum force (F_{max}) at human body and at R_f temperatures

Suture diameter (mm)	Body temperature			R_f		
	K (N/mm)	d_f (μm)	F_{max} (N)	K (N/mm)	d_p (μm)	F_{max} (N)
2	25.6	322.5	7.9	8.0	227.7	2.0
3	15.9	332.7	5.1	7.9	315.2	2.7
4	6.5	646.8	3.5	4.9	483.1	2.2

presents a higher stiffness compared to commercially available knotted sutures [23]. Furthermore, the pseudoplastic deformation given to the suture while in the R-phase state is advantageous for convenient suture removal. As a general rule, suture removal can be achieved simply by lowering the temperature of both the suture and the surrounding environment to a value below R_f. At this point, a physician can simply open the suture arms and pull the device out with forceps. The simple geometry of the device prevents issues such as manual knotting, which is achieved through self-closing instead. Furthermore, the risk of scarring and infection is lessened due to the absence of stainless steel needles. Therefore, compared to the traditional approach (Table 1), the new NiTi suturing operation is radically reduced to two steps: (1) wire

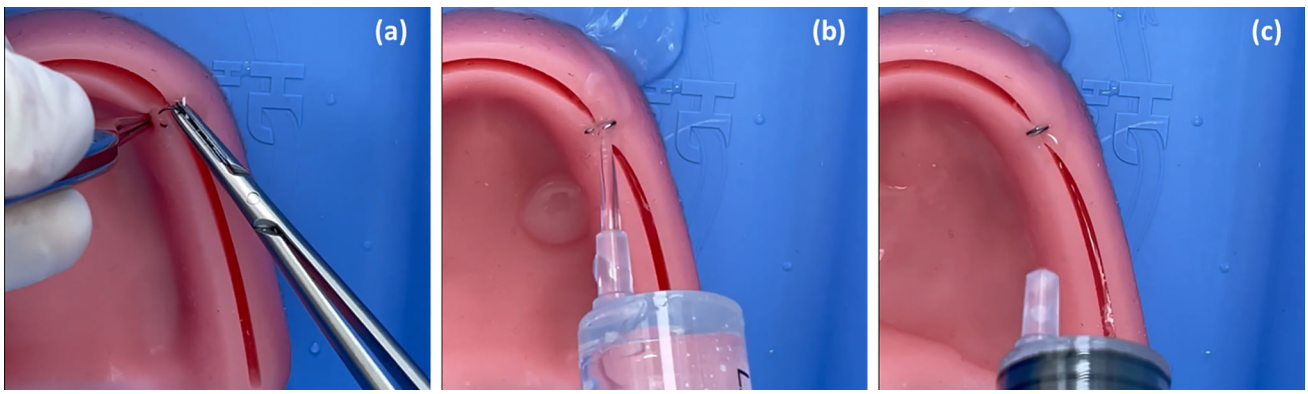

Fig. 7 Photographs of suturing steps with the Φ_{S2} suture on a silicon oral model: **a** suture introduction; **b** and **c** self-knotting. Φ_{S2}: suture with closed configuration diameter of 2 mm

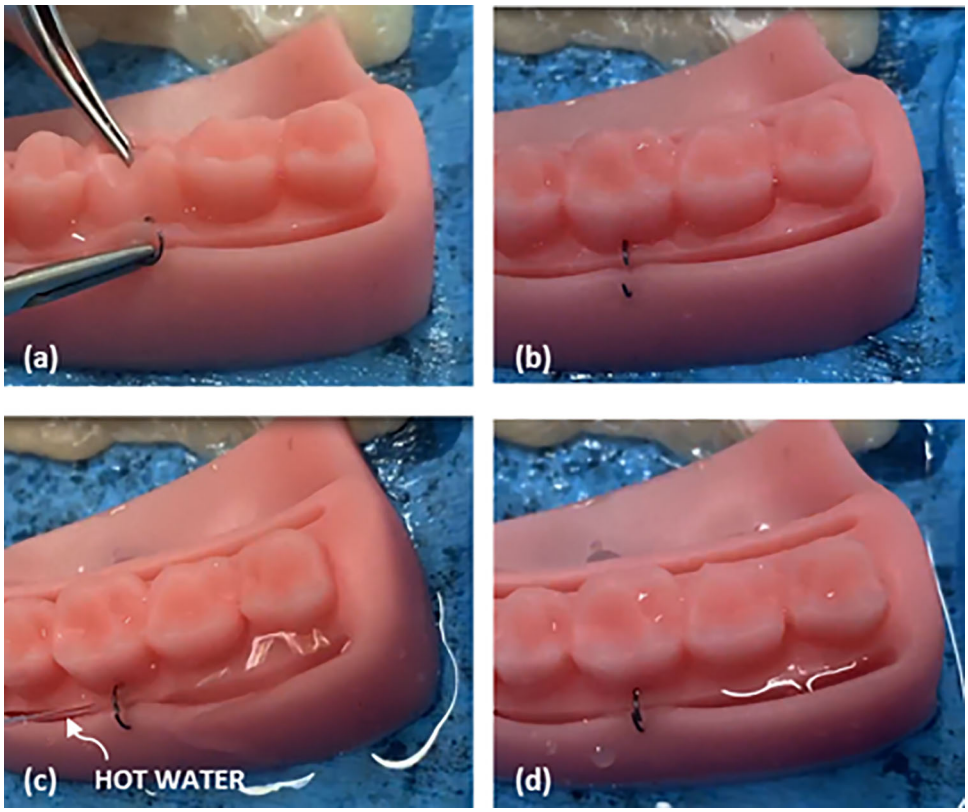

Fig. 8 Photographs of suturing steps with Φ_{S3} sutures on a silicon oral model: **a** and **b** suture introduction; **c** and **d** self-knotting. Φ_{S3}: suture with closed configuration diameter of 3 mm

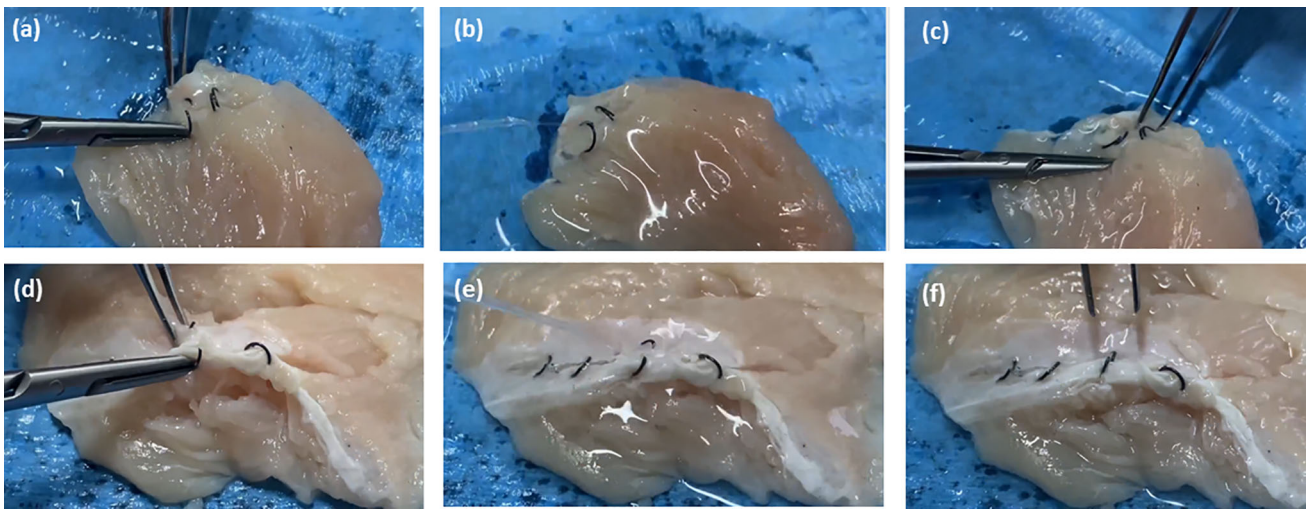

Fig. 9 Photographs of suturing steps on a commercial animal tissue: **a–c** Φ_{S4} suture and **d–f** Φ_{S3} suture. Φ_{S4}: suture with closed configuration diameter of 4 mm; Φ_{S3}: suture with closed configuration diameter of 3 mm

introduction and (2) closure of the knot with warm water. Moreover, another important advantage of the novel suture described here is that the closing force does not depend on the surgeon's skill, since the tightening is exclusively ascribed to the self-accommodation of the material during the phase transition while heated. Therefore, the absence of manual knotting permits uniform strength along the suture path.

Assuming that the suture exerts a uniaxial tensile test on the tissue during closing, it is possible to determine whether the static force generated can damage the soft tissue to which it is anchored. For instance, several studies have investigated the failure properties of soft tissues. Ayyalasomayajula et al. [38] studied these failure properties under a uniaxial tensile test of the adventitia layer of the descending abdominal aorta.

They observed failure stress values of 0.96 and 0.86 MPa for circumferential and longitudinal specimens respectively obtained from the aorta. Similarly, García-Herrera et al. [39] characterized the mechanical responses of samples obtained from the ascending aortic wall and found failure stress values of 1.20 and 0.66 MPa for circumferential and longitudinal samples, respectively.

In addition, Bonaldi et al. [40] studied the failure mechanism of human fascia lata using uniaxial tensile tests and found failure stress values ranging between 0.5 and 12 MPa. Morrow et al. [41] also used tensile tests of rabbit extensor digitorum longus muscle to assess the mechanical response and found a failure stress value of 0.163 MPa. Similarly, a study by Petersen et al. [42] found a cervical tissue failure stress value of 1.8 MPa when studying its mechanical response using a uniaxial tensile test. Finally, Stavropoulou et al. [43] tested the tensile stress of esophageal tissue in different layers (i.e., mucosa–submucosa, inner muscle, and outer muscle), both within the esophagus and in other nearby regions (i.e., cervical, thoracic, and abdominal). They found failure stress values ranging from 0.13 MPa (for a circumferential sample of the outer muscle of the esophagus abdominal region) to 1.7 MPa (for a longitudinal sample of the outer muscle of the esophagus abdominal region).

By applying the suture closing force to these tissues and examining the stresses generated in them, it is possible to determine that in most cases the novel suture described here would generate an axial stress lower than the failure stress value. However, there are rare cases in which the suture could damage nearby tissues. For example, the 2-mm suture, which exerts a 2.3 N closing force, would generate an axial stress of 0.9 MPa as estimated using the method of the human fascia lata sample examined by Bonaldi et al. [40]. This value is within the range of failure stresses obtained for this tissue as measured by tensile tests. Therefore, it is fundamental to properly design the suture according to the tissue that the suture will be applied to. No unique geometric configuration of the suture (i.e., diameter of the wire and/or diameter of the closed suture) can be used in all tissues.

Compared to the NiTi suture presented in [23], the new NiTi device has the advantage of being needle-less. The absence of stainless steel needles significantly decreases the waste produced by suturing. Another key advantage is that a version of the novel NiTi suture can be used for microsurgery. Table 4 lists key advantages of the NiTi and barbed sutures. This list shows that the NiTi material offers significant improvements for surgical suturing. Nevertheless, to properly compare this suture design with commercially available sutures (e.g., with respect to suturing speed, cost, complication rate, etc.), a large amount of clinical data must be obtained [9, 44]. However, until the novel suture described here is available on the market, no quantitative comparison with other types of sutures is possible.

Table 4 Advantages of NiTi and barbed sutures

Advantages	Previous NiTi suture [23]	Current NiTi suture	Barbed suture [9–11]
No knots	×	×	×
No handling	×	×	×
No needle		×	
No waste		×	
Gradual self-closing	×	×	
Implantable	×	×	
Micro- + macro-surgery	×	×	
Microsurgery (dedicated)		×	

Figure 10 reports a list of benefits conferred by the new device, not only to the patient, but also to the surgeon and the hospital. However, in addition to its numerous benefits, the novel suture described here has some limitations. The main concern involves its novelty, since the medical staff must use it despite its use being quite different from traditional suturing. Although NiTi materials are already well-known in the medical field (due to NiTi archwires, stents, and staples, among other devices), the mechanical functioning of the suture and its handling may be obstacles for adoption and acceptance. Another issue concerns the maintenance of the correct open configuration at each stage of the suture lifecycle, from production to use in the operating room. In fact, given its known phase transformation temperatures, it may be necessary to adopt special packaging to keep the device at temperatures below A_s to avoid unexpected shape recovery before medical use.

In conclusion, in this study we present a proof of concept of a medical device tested in a laboratory environment that is not ready to be used in clinical environments. Further experimentation is required to further study this NiTi device and to achieve a technology readiness level of nine.

Conclusions

This study presents a proof-of-concept design of an innovative surgical suture consisting of a very short NiTi shape memory alloy wire, opportunely shaped to enable the self-knotting at convenient temperatures.

The main conclusions can be summarized as follows:

1. The NiTi shape memory alloy is a suitable material for developing biomedical devices aimed at simplifying surgical procedures.

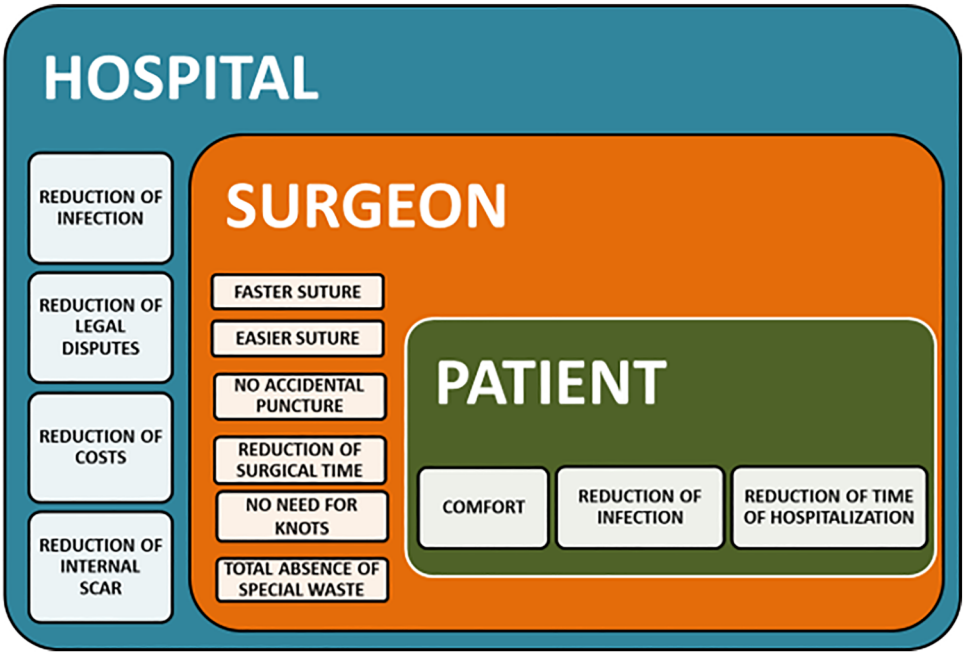

Fig. 10 Benefits of the novel NiTi suture device for patients, surgeons, and hospitals

2. The presented suture has the advantage of being self-tightening and needle-less. Consequently, the steps involved in the knotting procedure are drastically reduced. Nevertheless, to determine whether the overall suturing time is decreased, it is fundamental to obtain clinical data, which at the current stage is not possible. In any case, suturing using the novel suture device is reduced to two steps: wire introduction and the closure of the knot with warm water.
3. The device exploits the R-phase. We found that the R-phase enables the suture to maintain proper deformation during handling until correctly positioned within the tissue. The R-phase is also useful for suture removal.
4. Novel characteristics ascribed to the properties of the NiTi alloy and the simple design of this suture device include reduced risk of inflammatory reaction and less waste. These are important benefits for patients, surgeons, and hospitals alike.
5. During the closing process, the suture may generate a stress field that is potentially dangerous for the surrounding tissue. Therefore, it is fundamental to properly design the geometry of this device based on the mechanical properties of the tissue to be sutured. For example, computational analysis may enable determination of the ideal geometric configuration of the suture (e.g., the best wire diameter and/or closed suture diameter to be adopted).

Acknowledgements The authors would like to thank Trafilspec ITS (Castelmarte-Como-Italy) for the supply of the drawn NiTi wire and its R&D team directed by Mr. Emanuele Pina for the technical support in the validation tests. Funding was provided by Regione Lombardia (Grant No. BANDO MISE Brevetti+ N. BRE0000721).

Author contributions AN was involved in data curation, formal analysis, investigation, methodology, validation, visualization, writing—original draft, and writing—review and editing. DN was involved in data curation, formal analysis, investigation, writing—original draft, and writing—review and editing. EB was involved in investigation and methodology. VD was involved in conceptualization, funding acquisition, investigation, methodology, project administration, resources, supervision, validation, visualization, and writing—original draft.

Declarations

Conflict of interest The authors declare that they have no conflict of interest.

Ethical approval This study does not contain any studies with human or animal subjects performed by any of the authors.

References

1. Robinson JK, Hanke CW, Siegel DM et al (2015) Surgery of the Skin: Procedural Dermatology. Elsevier, London
2. Watkins FH, London SD, Neal JG et al (1997) Biomechanical performance of cutting edge surgical needles. J Emerg Med 15(5):679–685. https://doi.org/10.1016/s0736-4679(97)00149-2
3. Chu CC (2013) Types and properties of surgical sutures. In: King MW, Gupta BS, Guidoin R (Eds.), Biotextiles as Medical Implants. Woodhead Publishing, Sawston, p.232–274. https://doi.org/10.1533/9780857095602.2.232
4. Ishii Y, Tahara S, Teramoto A et al (2014) Endoscopic endonasal skull base surgery: advantages, limitations, and our techniques to overcome cerebrospinal fluid leakage: technical note. Neurol Med Chir 54(12):983–990. https://doi.org/10.2176/nmc.st.2014-0081
5. Xue H, Yang ZJ, Liu J et al (2021) Continuous dural suturing for closure of grade 3 leaks after tumor removal via an endoscopic endonasal approach. Neurosurg Rev 44(1):373–380. https://doi.org/10.1007/s10143-019-01199-w
6. Malik MU, Aberle JC, Flitsch J (2012) CSF fistulas after transsphenoidal pituitary surgery—a solved problem? J Neurol Surg A Cent Eur Neurosurg 73(5):275–280. https://doi.org/10.1055/s-0032-1304808
7. Chen YK, Xu XH, Cao J et al (2022) Transsphenoidal surgery of giant pituitary adenoma: results and experience of 239 cases in a single center. Front Endocrinol 13:879702. https://doi.org/10.3389/fendo.2022.879702
8. Khan DZ, Ali AMS, Koh CH et al (2021) Skull base repair following endonasal pituitary and skull base tumour resection: a systematic review. Pituitary 24(5):698–713. https://doi.org/10.1007/s11102-021-01145-4
9. Song T, Kim TJ, Kim WY et al (2015) Comparison of barbed suture versus traditional suture in laparoendoscopic single-site myomectomy. Eur J Obstet Gynecol 185:99–102. https://doi.org/10.1016/j.ejogrb.2014.11.022
10. Contegiacomo A, Cina A, Di Stasi C et al (2020) Uterine myomas: endovascular treatment. Semin Ultrasound CT 42(1):13–24. https://doi.org/10.1053/j.sult.2020.07.002
11. Gardella B, Dominoni M, Lacobone AD et al (2018) What is the role of barbed suture in laparoscopic myomectomy? A meta-analysis and pregnancy outcome evaluation. Gynecol Obstet Invest 83:521–532. https://doi.org/10.1159/000488241
12. Ardovino M, Castaldi MA, Fraternali F et al (2013) Bidirectional barbed suture in laparoscopic myomectomy: clinical features. J Laparoendosc Adv Surg Tech 23(12):1006–1010. https://doi.org/10.1089/lap.2013.0103
13. Mann C, Berlth F, Hadzikusufovic E et al (2020) Minimally invasive esophagectomy: clinical evidence and surgical techniques. Langenbecks Arch Surg 405(8):1061–1067. https://doi.org/10.1007/s00423-020-02003-w
14. Carr RA, Molena D (2021) Minimally invasive esophagectomy: anastomotic techniques. Ann Esophagus 3:19. https://doi.org/10.21037/aoe-20-40
15. Xu QL, Li H, Zhu YJ et al (2020) The treatments and postoperative complications of esophageal cancer: a review. J Cardiothorac Surg 15(1):163. https://doi.org/10.1186/s13019-020-01202-2
16. Edmiston CE Jr, Krepel CJ, Wilson PJ et al (2008) Reducing the risk of surgical site infections: embracing basic and innovative risk reduction strategies. Healthc Infect 13(4):121–129. https://doi.org/10.1071/HI08033
17. Van Ramshorst GH, Nieuwenhuizen J, Hop WCJ et al (2010) Abdominal wound dehiscence in adults: development and validation of a risk model. World J Surg 34(1):20–27. https://doi.org/10.1007/s00268-009-0277-y
18. Metgud MC, Kataria A, Nadipally SR et al (2020) Incidence of wound dehiscence following obstetric and gynecological surgeries at a tertiary care hospital: a retrospective study. J South Asian Federation Obst Gyn 12(2):73–78. https://doi.org/10.5005/jp-journals-10006-1763
19. Emori TG, Gaynes RP (1993) An overview of nosocomial infections, including the role of the microbiology laboratory. Clin Microbiol Rev 6(4):428–432. https://doi.org/10.1128/CMR.6.4.428
20. Crosetti E, Caracciolo A, Arrigoni G et al (2019) Barbed suture in oral cavity reconstruction: preliminary results. Acta Otorhinolaryngol Ital 39(5):308–315. https://doi.org/10.14639/0392-100X-2130
21. Greenberg JA, Goldman RH (2013) Barbed suture: a review of the technology and clinical uses in obstetrics and gynecology. Rev Obstet Gynecol 6(3–4):107–115. https://doi.org/10.3909/riog0231
22. Lin YF, Lai S, Huang J et al (2016) The efficacy and safety of knotless barbed sutures in the surgical field: a systematic review and meta-analysis of randomized controlled trials. Sci Rep 6:23425. https://doi.org/10.1038/srep23425
23. Nespoli A, Dallolio V, Villa E et al (2015) A new design of a Nitinol ring-like wire for suturing in deep surgical field. Mater Sci Eng C 56:30–36. https://doi.org/10.1016/j.msec.2015.06.009
24. Petrini L, Migliavacca F (2011) Biomedical applications of shape memory alloys. J Metall 2011:1–15. https://doi.org/10.1155/2011/501483
25. Wen CS, Yu XJ, Zeng W et al (2018) Mechanical behaviors and biomedical applications of shape memory materials: a review. AIMS Mater Sci 5(4):559–560. https://doi.org/10.3934/matersci.2018.4.559
26. Barbarino S, Saavedra Flores EI, Ajaj RM et al (2014) A review on shape memory alloys with applications to morphing aircraft. Smart Mater Struct 23(6):1–19. https://doi.org/10.1088/0964-1726/23/6/063001
27. McDonald SL (1991) Shape memory alloy applications in space systems. Mater Des 12(1):29–32. https://doi.org/10.1016/0261-3069(91)90089-M
28. Dutta SC, Majumder R (2019) Shape memory alloy (SMA) as a potential damper in structural vibration control. In: Hloch S, Klichová D, Krolczyk G et al (Eds.), Advances in Manufacturing Engineering and Materials. Springer, Cambridge, p.485–492. https://doi.org/10.1007/978-3-319-99353-9_51
29. Borlandelli E, Scarselli D, Nespoli A et al (2015) Design and experimental characterization of a NiTi-based, high-frequency, centripetal peristaltic actuator. Smart Mater Struct 24(3):035008. https://doi.org/10.1088/0964-1726/24/3/035008
30. Nespoli A, Rigamonti D, Riva M et al (2016) Study of pseudoelastic systems for the design of complex passive dampers: static analysis and modeling. Smart Mater Struct 25(10):105001. https://doi.org/10.1088/0964-1726/25/10/105001
31. Chen QF, Zuo XB, Wang LM et al (2006) NiTi wire as a superelastic damping material in structural engineering. Mater Sci Eng A 438:1089–1092. https://doi.org/10.1016/j.msea.2006.02.196
32. Nespoli A, Bassani E, Della Torre D et al (2017) An experimental study on pseudoelasticity of a NiTi-based damper for civil applications. Smart Mater Struct 26(10):105041. https://doi.org/10.1088/1361-665X/aa882e
33. Nespoli A, Villa E, Bergo L et al (2015) DSC and three-point bending test for the study of the thermo-mechanical history of NiTi and NiTi-based orthodontic archwires. J Therm Anal Cal 120(2):1129–1138. https://doi.org/10.1007/s10973-015-4441-3
34. Otsuka K, Ren X (2005) Physical metallurgy of Ti–Ni-based shape memory alloys. Proc Mater Sci 50(5):511–678. https://doi.org/10.1016/j.pmatsci.2004.10.001
35. Dallolio V (2020) Suture Device. EP Patent 3474754B1
36. Holton A, Walsh E, Anayiotos A et al (2002) Comparative MRI compatibility of 316L stainless steel alloy and nickel-titanium alloy

stents. J Cardiovasc Magn Reson 4(4):423–430. https://doi.org/10.1081/jcmr-120016381
37. Sund-Levander M, Forsberg C, Wahren LK (2002) Normal oral, rectal, tympanic and axillary body temperature in adult men and women: a systematic literature review. Scand J Caring Sci 16(2):122–128. https://doi.org/10.1046/j.1471-6712.2002.00069.x
38. Ayyalasomayajula V, Pierrat B, Badel P (2023) Failure properties and microstructure of porcine aortic adventitia: fiber level damage vs tissue failure. BioRxiv. https://doi.org/10.1101/2023.03.13.531658
39. García-Herrera CM, Atienza JM, Rojo FJ et al (2012) Mechanical behaviour and rupture of normal and pathological human ascending aortic wall. Med Biol Eng Comput 50(6):559–566. https://doi.org/10.1007/s11517-012-0876-x
40. Bonaldi L, Berardo A, Pirri C et al (2023) Mechanical characterization of human fascia lata: uniaxial tensile tests from fresh-frozen cadaver samples and constitutive modelling. Bioengineering 10(2):226. https://doi.org/10.3390/bioengineering10020226
41. Morrow DA, Donahue TLH, Odegard GM et al (2008) Transversely isotropic tensile material properties of skeletal muscle tissue. J Mech Behav Biomed Mater 3(1):124–129. https://doi.org/10.1016/j.jmbbm.2009.03.004
42. Petersen LK, Vogel I, Oxlundb H et al (1997) No effects of human relaxing on the active and passive biomechanical properties of isolated cervical specimens from nonpregnant women. Eur J Obstet Gynecol Reprod Biol 73(2):183–187. https://doi.org/10.1016/s0301-2115(97)02732-2
43. Stavropoulou EA, Dafalias YF, Sokolis DP (2012) Biomechanical behavior and histological organization of the three-layered passive esophagus as a function of topography. J Eng Med 226(6):477–490. https://doi.org/10.1177/0954411912444073
44. Smith EL, DiSegna ST, Shukla PY et al (2014) Barbed versus traditional sutures: closure time, cost, and wound related outcomes in total joint arthroplasty. J Arthroplasty 29(2):283–287. https://doi.org/10.1016/j.arth.2013.05.031